INTERNATIONAL JOURNAL FOR NUMERICAL METHODS IN FLUIDS
Int. J. Numer. Meth. Fluids 2009; **59**:387–403
Published online 28 April 2008 in Wiley InterScience (www.interscience.wiley.com). DOI: 10.1002/fld.1820

On pressure separation algorithms (PSepA) for improving the accuracy of incompressible flow simulations

S. Turek*, †, A. Ouazzi and J. Hron

Institute for Applied Mathematics, TU Dortmund, Germany

SUMMARY

We investigate a special technique called 'pressure separation algorithm' (PSepA) (see *Applied Mathematics and Computation* 2005; **165**:275–290 for an introduction) that is able to significantly improve the accuracy of incompressible flow simulations for problems with large pressure gradients. In our numerical studies with the computational fluid dynamics package FEATFLOW (www.featflow.de), we mainly focus on low-order Stokes elements with nonconforming finite element approximations for the velocity and piecewise constant pressure functions. However, preliminary numerical tests show that this advantageous behavior can also be obtained for higher-order discretizations, for instance, with Q_2/P_1 finite elements. We analyze the application of this simple, but very efficient, algorithm to several stationary and nonstationary benchmark configurations in 2D and 3D (driven cavity and flow around obstacles), and we also demonstrate its effect to spurious velocities in multiphase flow simulations ('static bubble' configuration) if combined with *edge-oriented*, resp., *interior penalty* finite element method stabilization techniques. Copyright © 2008 John Wiley & Sons, Ltd.

Received 31 May 2007; Revised 4 March 2008; Accepted 5 March 2008

KEY WORDS: pressure separation; incompressible Navier–Stokes equations; finite elements; multiphase; driven cavity; edge-oriented stabilization

1. MOTIVATION

The improvement in numerical simulation techniques for the incompressible Navier–Stokes equations w.r.t. accuracy, flexibility and robustness still belongs to the important and challenging numerical tasks nowadays. Besides the search for 'better' LBB-stable approximations for pressure and velocity, resp., corresponding stabilization techniques for the numerical treatment of higher Reynolds numbers and for higher-order time discretizations, concepts for local adaptivity in space

*Correspondence to: S. Turek, Institute for Applied Mathematics, TU Dortmund, Germany.
†E-mail: ture@featflow.de

Contract/grant sponsor: German Research Association (DFG); contract/grant numbers: TU 102/11-3 (FOR493), TU 102/21-1

and time belong to the most common techniques, which are typically under research. In this paper, we demonstrate as an alternative how to increase the resulting accuracy by a simple trick, namely by 'pressure separation algorithms' (PSepA), which are designed for flow situations that are dominated by the pressure gradient or higher-order pressure derivatives.

We illustrate the underlying idea, which was originally described in [1] and quite recently in the paper [2], containing numerical results for problems with analytical solutions. In our contribution, we demonstrate the advantageous behavior of this approach for more realistic computational fluid dynamics (CFD) configurations and provide results from detailed numerical studies. To do so, we focus on the (stationary) Navier–Stokes equations for an incompressible fluid in a bounded domain Ω, which read as

$$\mathbf{u}\cdot\nabla\mathbf{u}-\nu\Delta\mathbf{u}+\nabla p=\mathbf{f},\quad \operatorname{div}\mathbf{u}=0 \tag{1}$$

where $\mathbf{u}$ is the fluid velocity, p the pressure, ν the kinematic viscosity, and $\mathbf{f}$ the body force. Moreover, corresponding boundary conditions on $\partial\Omega$ have to be specified depending on the model problems.

If, as usually, the norm in $(L^2(\Omega))^N, N=2,3$, is denoted by $\|\cdot\|_{0,\Omega}$, the norm in $(H^k(\Omega))^N$ by $\|\cdot\|_{k,\Omega}$ and the semi-norm in $(H^k(\Omega))^N$ by $|\cdot|_{k,\Omega}$, then the typical velocity error estimation for approximating the Navier–Stokes equations with finite elements of order k for the velocity and (at least) of order $k-1$ for the pressure can be expressed as follows (see [3])

$$h|\mathbf{u}-\mathbf{u}_h|_{1,\Omega}+\|\mathbf{u}-\mathbf{u}_h\|_{0,\Omega}\leqslant Ch^{k+1}\left\{|\mathbf{u}|_{k+1,\Omega}+\frac{1}{\nu}|p|_{k,\Omega}\right\} \tag{2}$$

where $\mathbf{u}_h$ is the corresponding finite element approximation of (1). Now, consider the following problem instead of (1) (see [2]):

$$\mathbf{u}\cdot\nabla\mathbf{u}-\nu\Delta\mathbf{u}+\nabla\tilde{p}=\mathbf{f}-\nabla p_{\text{sep}},\quad \operatorname{div}\mathbf{u}=0 \tag{3}$$

where p_{sep} is a given function, and $\tilde{p}=p-p_{\text{sep}}$. Then, the corresponding *a priori* error estimate [2] reads as follows, which is the central observation for the following PSepA:

$$h|\mathbf{u}-\mathbf{u}_{\text{sep},h}|_{1,\Omega}+\|\mathbf{u}-\mathbf{u}_{\text{sep},h}\|_{0,\Omega}\leqslant Ch^{k+1}\left\{|\mathbf{u}|_{k+1,\Omega}+\frac{1}{\nu}|p-p_{\text{sep}}|_{k,\Omega}\right\} \tag{4}$$

Consequently, a significant improvement in the (*a priori*) error estimation is achieved if $|p|_{k,\Omega}/\nu$ is the dominant term in (2) and if $|p-p_{\text{sep}}|_{k,\Omega}\ll|p|_{k,\Omega}$. This situation typically occurs in flow configurations that are dominated by the pressure gradient or for small viscosity parameters such that the choice of p_{sep} as a sufficiently 'good' approximation of the original pressure in (1) is desired. Typical variants for the choice of p_{sep} can be found in [2, 4]. Similar approaches, mostly in the context of multiphase flow problems that require special treatment of discontinuous pressure or in the case of pressure correction schemes, can be found in [5–11].

Here, we extend the prototypical studies in [2] by applying this approach in the finite element method (FEM) context for stationary and nonstationary problems, which all are of prototypical character, since they are based on typically well-known benchmark configurations on quite general meshes and for different Reynolds numbers. Altogether, we believe that these numerical studies elucidate the potential of this simple and cheap, but nevertheless effective, technique for a wide range of complex CFD problems.

DOI: 10.1002/fld

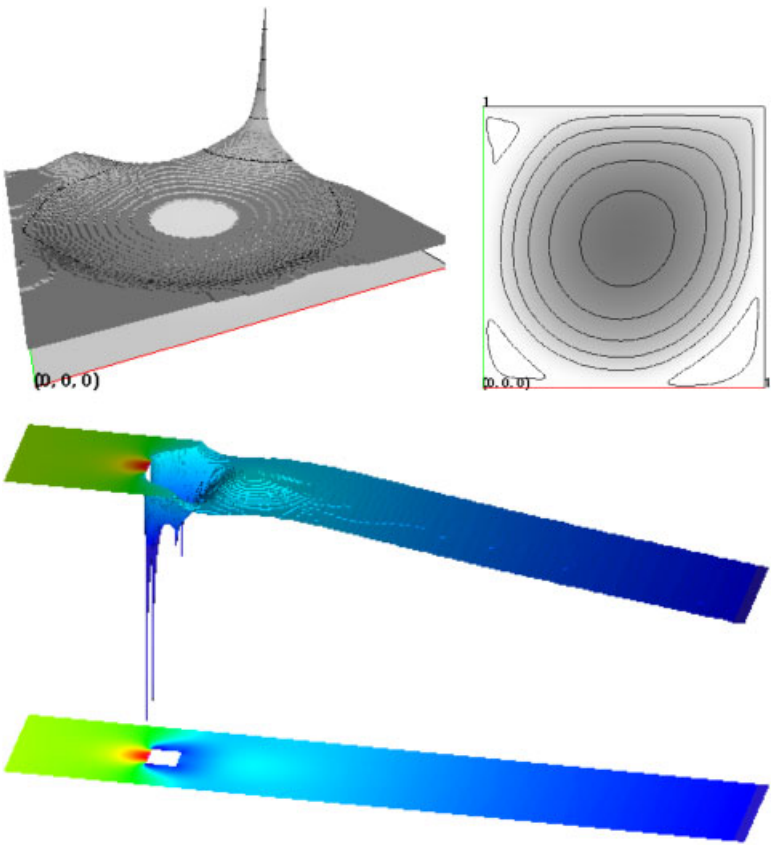

Figure 1. Singularity of the pressure for the 'driven cavity' configuration, together with the streamfunction (top), and for 'flow around a square' (bottom).

Prototypical configurations in single-phase CFD simulations, which are candidates for such flows with large pressure gradients, are problems with singularities, which are due to the geometry or boundary conditions. For instance, *driven cavity* problems with pressure singularities (see Figure 1) in the upper corners due to discontinuous boundary values for the velocity, or *flow around obstacles* settings with large pressure derivatives or even singularities near corners (see Figure 1), are typical flow settings that are natural candidates for *pressure separation*.

Another example is multiphase flow with surface tension as local external force, which in many cases leads to a discontinuous pressure, such that large norms of pressure derivatives naturally appear in *a priori* estimate (2). Moreover, spurious velocities appears near the interfaces (see Figure 2)—which are not restricted only to such free interface problems (see [12])—such that the question arises whether PSepA can improve the numerical accuracy and robustness in such examples too. For further improvement of the FEM solution in this case, we will use local mesh deformation techniques for grid alignment to accurately calculate the surface tension force and the curvature, and we will combine them with edge-oriented FEM stabilization techniques [13] that will essentially help to suppress such spurious oscillations (see Section 4).

DOI: 10.1002/fld

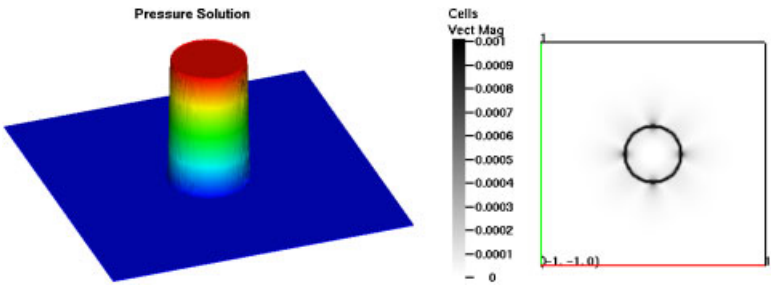

Figure 2. Pressure and resulting spurious velocity for a 'static bubble' configuration.

2. NUMERICAL AND ALGORITHMIC DETAILS

2.1. Discretization aspects

For the discretization, we consider a usual subdivision $T \in \mathscr{T}_h$ consisting of quadrilaterals/hexahedrals in the domain Ω, and we employ the nonconforming rotated multilinear $\tilde{Q}_1/Q_0$ finite element pair; however, the following algorithms can be applied to other finite element, finite difference or finite volume discretizations too. In our situation, the nodal values are the mean values of the velocity vector over the element edges, resp., element faces, and the mean values of the pressure over the elements (see [14] for more details).

There are two well-known situations for nonconforming FEM methods when severe numerical problems may arise: Firstly, the lack of coercivity for low-order approximations for symmetric deformation tensor formulations, mainly visible for small Re numbers. Secondly, for all standard discretization schemes in the case of convection dominated problems, numerical difficulties arise for instance for medium and high Re numbers or for the treatment of pure transport problems. Then, the standard Galerkin formulation usually fails and may lead to numerical oscillations and to convergence problems of the iterative solvers too (see [13, 15]). Among the stabilization methods existing in the literature for these types of problems, we use the one proposed in [13, 16], which is based on the penalization of the gradient jumps over element boundaries. In 2D, the additional stabilization term $\mathbf{Ju}$, acting only on the velocity $\mathbf{u}$ in the momentum equations, takes the following form (with $h_E = |E|$):

$$\langle \mathbf{Ju}, \mathbf{v} \rangle = \sum_{\text{edge E}} \max(\gamma \nu h_E, \gamma^* h_E^2) \int_E [\nabla \mathbf{u}] : [\nabla \mathbf{v}] \, \mathrm{d}s \tag{5}$$

and will be simply added to the original bilinear form in order to cure numerical instabilities when computing incompressible flow problems using low-order nonconforming finite elements. Moreover, only one generic stabilization term takes care of all mentioned instabilities (see [13] for more details).

The original method presented in (5) was driven by the desire to cure both instabilities for Korn's inequality and convection domination inherent in the approximate solutions. This least-squares term may be interpreted as a continuous high-order interior penalty method that can be formulated as a global minimization of the quadratic formulation, derived from the Stokes problem, for instance, with the constraint of the jump of the gradient being equal to zero. Hence, it can

DOI: 10.1002/fld

be seen as a manner of filtering the undesired spurious modes in the solution. Moreover, that explains the adequate results in the limit of inviscid flow if the stabilization according to (5) is applied (see [13] for the 'standing vortex' problem). Therefore, the objective is to generalize the mesh-dependent penalty parameter in (5) to provide improvements for two-phase flows with discontinuous pressure too.

2.2. Algorithmic realization of pressure separation

To reach where the semi-norm $|p-p_{\text{sep}}|_k$ is smaller than $|p|_k$, we try to set p_{sep} as an approximate solution to the unknown pressure p. This simply can be done by defining p_{sep}, for instance, via appropriate interpolation of the discrete solution p_h from the original problem (1). In the following, we denote by '$\text{NS}^{-1}(\mathbf{g})$' the solution to a discretized incompressible Navier–Stokes problem, for a given right-hand side $\mathbf{g}$, by *any* method, for instance, using a fully coupled approach or pressure correction, etc.

Then, the complete (stationary) PSepA, which can be also viewed as a basic step inside of a corresponding iterative procedure, reads as follows:

1. Step of PSepA:

0. Solve the original problem (1) and obtain $(\mathbf{u}_h^0, p_h^0)$ that means $(\mathbf{u}_h^0, p_h^0) = \text{NS}^{-1}(\mathbf{f})$.
1. Interpolate p_h^0 into any higher-order finite element space, at least consisting of piecewise linear, resp., bilinear functions, which leads to
$$p_{\text{sep},h} := I(p_h^0)$$
2. Calculate the new finite element solution to the modified Navier–Stokes equations (3) with $\mathbf{f}-\nabla p_{\text{sep},h}$ as the right-hand side:
$$(\tilde{\mathbf{u}}_h, \tilde{p}_h) := \text{NS}^{-1}(\mathbf{f}-\nabla p_{\text{sep},h})$$
3. Set the velocity $\mathbf{u}_h = \tilde{\mathbf{u}}_h$ and update the pressure p_h:
$$p_h = p_h^0 + \tilde{p}_h$$

If the initial pressure p_h^0 is obtained by solving the original Navier–Stokes equations with $\mathbf{f}$ as the right-hand side, this *almost doubles* the CPU times. Alternatively, the computation of p_h^0 can be based on an approximation p_{2h}, which is obtained in a hierarchical multigrid style on a coarser mesh level $2h$, for instance, or p_h^0 can be directly obtained from a previous Newton-like step, which is typically used in an outer loop for treating the nonlinearity. For a discussion of further variants for computing $p_{\text{sep},h}$, the reader is referred to [2]. Regarding the underlying finite element spaces, in our case the nonconforming Stokes element $\tilde{Q}_1/Q_0$, the intermediate pressure $p_{\text{sep},h}$ is taken as the linear interpolation of p_h into conforming bilinear elements; we also used the interpolation into the nonconforming space $\tilde{Q}_1$, which, however, gives qualitatively similar results.

Regarding the application of pressure separation in the case of the nonstationary Navier–Stokes equations with any time-stepping scheme, the same algorithm could be applied in each time step separately, leading again to approximately doubling the CPU times as upper bound. However, there is also the possibility of the following simplification that is based on the well-known idea of extrapolating the pressure in time.

DOI: 10.1002/fld

1. Step of nonstationary pressure separation:

0. Given $(\mathbf{u}_h^{n-1}, p_h^{n-1})$ as the solution from time step t^{n-1}
1. Interpolate p_h^{n-1} into any higher-order finite element space, at least consisting of piecewise linear, resp., bilinear functions, which leads to
$$p_{\mathrm{sep},h}^n := I(p_h^{n-1})$$
2. Calculate the new finite element solution at time t^n with $\nabla p_{\mathrm{sep},h}^n$ as part of the modified right-hand side:
$$(\tilde{\mathbf{u}}_h^n, \tilde{p}_h^n) := \mathrm{NS}^{-1}(\mathbf{f}^n - \nabla p_{\mathrm{sep},h}^n)$$
3. Set the velocity as $\mathbf{u}_h^n = \tilde{\mathbf{u}}_h^n$ and update the pressure p_h^n:
$$p_h^n = p_h^{n-1} + \tilde{p}_h^n$$

Remark
In step 2, we mean by 'NS^{-1}' again the solution to a corresponding generalized stationary Navier–Stokes problem at time step t^n, which now depends on the chosen time stepping. In our case, we assume a fully coupled, fully implicit approach that, however, can be easily extended to pressure correction and pressure projection methods or other semi-implicit variants. Furthermore, the approximative pressure $p_{\mathrm{sep},h}^n$ can be easily taken as a higher-order extrapolation in time, for instance, via $p_{\mathrm{sep},h}^n = I(2p_h^{n-1} - p_h^{n-2})$ in the case of equidistant time steps, which should lead to improved approximation properties due to higher temporal accuracy with almost the same numerical effort.

3. NUMERICAL ANALYSIS

The goal of the following examples is to analyze numerically the improvement w.r.t. the resulting accuracy of velocity and pressure using the proposed PSepA for several prototypical flow configurations. Here, we restrict our studies to the shown 'simple' variants, which means that the subsequent solution to two problems in the steady case and the constant extrapolation of $p_{\mathrm{sep},h}^n = I(p_h^{n-1})$ backwards in time, in order to show the potential of these approaches regarding the numerical accuracy, not considering the related necessary aspects of numerical efficiency which in the steady test cases can be roughly estimated by a factor of 2. However, it is obvious that there exist improved techniques for calculating $p_{\mathrm{sep},h}$, which might further improve the numerical efficiency.

3.1. Analytical solution

The first example is a 2D test on the unit square for two different Reynolds numbers $Re = 1$ and 1000 and analytically given velocity $\mathbf{u} = (u_1, u_2)$ and pressure p as defined by the following polynomials:

$$\begin{aligned} u_1(x,y) &= 2x^2(1-x^2)(y(1-y)^2 - y^2(1-y)) \\ u_2(x,y) &= 2y^2(1-y^2)(x(1-x)^2 - x^2(1-x)) \\ p(x,y) &= c(x^3 - y^3 - 0.5) \end{aligned} \tag{6}$$

DOI: 10.1002/fld

The constant c is varied to obtain the corresponding *a priori* error estimate in (2) which is dominated by the pressure gradient and to see its impact on the accuracy of the computed solution. The right-hand side $\mathbf{f}$ is chosen such that $(\mathbf{u}, p)$ satisfy the stationary Navier–Stokes equations for the given Reynolds numbers. In Table I, we give the corresponding L^2-norm and H^1-norm of the velocity error and the L^2-norm for the pressure error on different mesh levels: 'Level n' denotes the n-times equidistantly refined unit square. As expected, both the 'high Reynolds number case' and the increase in the absolute pressure values have directly influenced the computed velocity error: Firstly, the error scales with the Reynolds number Re, and, secondly, the constant c increases the error since the pressure magnitude and hence its gradient are scaled with c. However, both dependencies influence the error only via the so-called error constant whereas the asymptotics w.r.t. the mesh size h remains the same. Nevertheless, it is obvious that the velocity errors are significantly improved by the PSepA (Table I).

Table I. Velocity errors due to $\|\mathbf{u}-\mathbf{u}_h\|_0$ and $|\mathbf{u}-\mathbf{u}_h|_1$, and pressure error $\|p-p_h\|_0$.

	Without pressure separation			With pressure separation		
Level	$\|\mathbf{u}-\mathbf{u}_h\|_0$	$\|\mathbf{u}-\mathbf{u}_h\|_{1,h}$	$\|p-p_h\|_0$	$\|\mathbf{u}-\mathbf{u}_h\|_0$	$\|\mathbf{u}-\mathbf{u}_h\|_{1,h}$	$\|p-p_h\|_0$
$Re=1,\ c=1$						
4	0.01320627	0.21977997	0.0428970	0.00407523	0.07914281	0.0448510
5	0.00332730	0.11060943	0.0213872	0.00093228	0.03681914	0.0219279
6	0.00083443	0.05545565	0.0106808	0.00022132	0.01766485	0.0108244
7	0.00020887	0.02776021	0.0053380	5.3792E−05	0.00863829	0.0053753
8	5.2246E−05	0.01388741	0.0026686	1.3252E−05	0.00426955	0.0026781
9	1.3064E−05	0.00694537	0.0013342	3.2879E−06	0.00212224	0.0013366
$Re=1,\ c=1000$						
4	10.7625546	173.711219	0.0428585	2.00796426	35.9718175	0.0449270
5	2.93779513	95.2942924	0.0213830	0.38075240	13.6844735	0.0219383
6	0.77022584	50.1414941	0.0106804	0.06983640	5.02810125	0.0108258
7	0.19738275	25.7520552	0.0053380	0.01258139	1.81319313	0.0053754
8	0.04997221	13.0541961	0.0026686	0.00224555	0.64752019	0.0026781
9	0.01257281	6.57264895	0.0013342	0.00039888	0.23009497	0.0013366
$Re=1000,\ c=1$						
4	2.56237929	27.0587977	0.0427753	0.37903284	6.77388344	0.0453306
5	0.96556353	23.0817867	0.0213682	0.11457742	4.11517335	0.0220339
6	0.34447421	18.6515627	0.0106783	0.03155326	2.27133044	0.0108454
7	0.11699463	13.7212946	0.0053377	0.00775593	1.11769202	0.0053789
8	0.03685431	9.02403558	0.0026686	0.00171123	0.49209582	0.0026787
9	0.01063014	5.36395474	0.0013342	0.00054886	0.19847427	0.0013367
$Re=1000,\ c=1000$						
4	264.699897	1185.01441	0.0433642	15.4317586	269.340443	0.0454205
5	147.874546	1122.20719	0.0214613	5.43204942	189.104707	0.0220733
6	76.8259785	1035.76326	0.0106911	1.83832538	131.945249	0.0108609
7	33.1379928	952.824272	0.0053391	0.63121919	90.9434163	0.0053842
8	10.6143169	891.529162	0.0026688	0.21236541	61.2296913	0.0026803
9	3.08294602	827.562355	0.0013343	0.06854484	39.5259910	0.0013371

DOI: 10.1002/fld

3.2. Driven cavity

Driven cavity flows represent a common standard benchmark for incompressible CFD codes and therefore we also present corresponding results for different Reynolds numbers (see [17] for a description of the problems settings). Furthermore, this problem seems to be an ideal test configuration for the pressure separation since the solution is less regular, which is due to the pressure singularity in the corner (since the velocity is discontinuous at the upper corners). Here, we present results for the *kinetic energy* $(1/2)\int_\Omega \|\mathbf{u}\|^2 \mathrm{d}x$ as the benchmark quantity that also has been used in [17, 18]. (Remark: So far, there is *no* reference solution for the considered Re numbers in the literature; however, comparing with [17, 18] indicates that the reference values behave approximately like $4.45-2$ for $Re=1000$ and $4.74-2$ for $Re=5000$.) We list in Table II the values for the kinetic energy, for a regular mesh and for an adapted one near the corners

Table II. Driven cavity results for $Re=1000$ and 5000.

		Energy	
Level	Cells	Without pressure separation	With pressure separation
Structured mesh			
$Re=1000$			
4	1024	4.255446720666505E−02	4.809523177616493E−02
5	4096	4.292753746090640E−02	4.582827797164316E−02
6	16384	4.354483303998137E−02	4.484310164052527E−02
7	65536	4.409022680894554E−02	4.459201173310999E−02
8	262144	4.436728290764166E−02	4.453541193883628E−02
9	1048576	4.447217597338023E−02	4.452227397784055E−02
$Re=5000$			
4	1024	4.744206618103668E−02	6.178545053709494E−02
5	4096	4.542745327131271E−02	5.596863706593847E−02
6	16384	4.394207364279471E−02	5.019652320714556E−02
7	65536	4.462170416774443E−02	4.802028792765253E−02
8	262144	4.589567777376605E−02	4.754149961543417E−02
9	1048576	4.677138548602210E−02	4.745519215584770E−02
Unstructured mesh			
$Re=1000$			
4	3392	3.937830914695982E−02	4.258603278981851E−02
5	13568	4.200638598599166E−02	4.399538203747823E−02
6	54272	4.343367659646590E−02	4.442539201306887E−02
7	217088	4.410374815761506E−02	4.451194162495991E−02
8	868352	4.437769488742017E−02	4.452067552798117E−02
9	3473408	4.447552512831641E−02	4.451922842679222E−02
$Re=5000$			
4	3392	3.694454761504827E−02	4.478929109363260E−02
5	13568	3.875516662905162E−02	4.519893868737240E−02
6	54272	4.160819937746986E−02	4.621377280452104E−02
7	217088	4.428310545723057E−02	4.712166739526875E−02
8	868352	4.596571822224903E−02	4.741444989451889E−02
9	3473408	4.683499558639783E−02	4.745377227286869E−02

DOI: 10.1002/fld

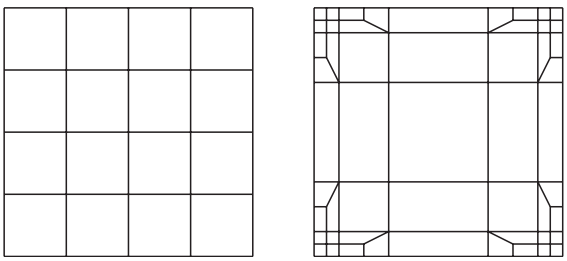

Figure 3. Two different coarse meshes for 'driven cavity'.

(see Figure 3). As can be seen in Table II, almost grid-independent results are achieved for the kinetic energy, at least for the PSepA approach. It is also seen that much better results can be obtained on coarse meshes with pressure separation in comparison with the standard approach.

3.3. Flow around obstacles

Flow around obstacles of different shapes is another adequate configuration to analyze the effectiveness of pressure separation not only w.r.t. the accuracy of the velocity but also regarding the pressure since the quantities of interest are the lift C_{lift} and the drag C_{drag} coefficients

$$C_{\text{lift}} = -C \int_S \left(\nu \frac{\partial \mathbf{v}_t}{\partial \mathbf{n}} \mathbf{n}_x + p \mathbf{n}_y \right) \mathrm{d}s, \quad C_{\text{drag}} = C \int_S \left(\nu \frac{\partial \mathbf{v}_t}{\partial \mathbf{n}} \mathbf{n}_y - p \mathbf{n}_x \right) \mathrm{d}s \tag{7}$$

where S is the contact line, resp., area of the obstacle with the fluid, and C is a scaling constant. The computation of the surface integrals in (7) can also be obtained using related volume integrals due to the weak formulations in FEM approaches. We consider functions $\mathbf{v}_d \in (H^1(\Omega))^N$ and $\mathbf{v}_l \in (H^1(\Omega))^N$ with

$$\mathbf{v}_{d|S} = (e_1, 0)^{\mathrm{T}}, \quad \mathbf{v}_{d|\bar{\Omega}-S} = \mathbf{0} \quad \text{and} \quad \mathbf{v}_{l|S} = (0, e_2)^{\mathrm{T}}, \quad \mathbf{v}_{l|\bar{\Omega}-S} = \mathbf{0} \tag{8}$$

where e_i is the ith component of the unity. Then, the corresponding expression using volume integrals [19] reads

$$\begin{aligned} C_{\text{lift}} &= -C((\nu \nabla \mathbf{u}, \nabla \mathbf{v}_l) - (p, \nabla \cdot \mathbf{v}_l)) \\ C_{\text{drag}} &= -C((\nu \nabla \mathbf{u}, \nabla \mathbf{v}_d) - (p, \nabla \cdot \mathbf{v}_d)) \end{aligned} \tag{9}$$

with $(\cdot, \cdot)$ denoting the inner product in $(L^2(\Omega))^N, N = 2, 3$. This problem corresponds to well-known benchmark configurations and has been described in [14, 20]. Two different obstacles, cylinders with circular and with square cross section, are considered in 2D and 3D. The coarse meshes for the 2D case are shown in Figure 4, whereas the corresponding 3D coarse mesh is derived from the 2D grid by extrusion in the z-direction with equidistant layers (Table III).

In the case of flow around a 2D cylinder, the solution is quite smooth and not dominated by the pressure gradient, which seems to be the reason why the PSepA does not essentially improve the solution quality, at least for the low Reynolds number cases $Re = 20$ and 50. However, in the 3D case [19, 21], the pressure separation brings significantly more improvement to the solution, particularly for the lift coefficient (see Table IV).

DOI: 10.1002/fld

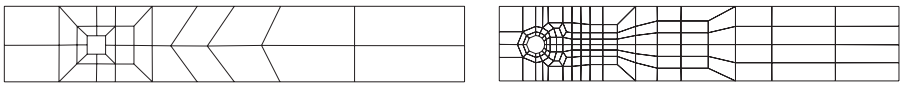

Figure 4. Coarse meshes for the 'flow around obstacle' configurations in 2D.

Table III. Flow around a 2D cylinder.

		Without pressure separation		With pressure separation	
Level	Cells	C_{drag}	C_{lift}	C_{drag}	C_{lift}
Force					
Re = 20/*reference values*: $C_{\text{drag}} \approx 5.580, C_{\text{lift}} \approx 0.0106$					
3	4264	0.56012E+01	0.96490E−02	0.56206E+01	0.10498E−01
4	16848	0.55803E+01	0.10143E−01	0.55703E+01	0.10350E−01
5	66976	0.55789E+01	0.10435E−01	0.55707E+01	0.10462E−01
6	267072	0.55793E+01	0.10559E−01	0.55747E+01	0.10548E−01
7	1066624	0.55795E+01	0.10601E−01	0.55771E+01	0.10588E−01
8	4263168	0.55795E+01	0.10614E−01	0.55783E+01	0.10605E−01
Re = 50/*reference values*: $C_{\text{drag}} \approx 3.694, C_{\text{lift}} \approx -0.0107$					
3	4264	0.38109E+01	−0.11007E−01	0.38136E+01	−0.11184E−01
4	16848	0.37237E+01	−0.10959E−01	0.37041E+01	−0.11045E−01
5	66976	0.37013E+01	−0.10794E−01	0.36897E+01	−0.10860E−01
6	267072	0.36961E+01	−0.10749E−01	0.36908E+01	−0.10786E−01
7	1066624	0.36949E+01	−0.10741E−01	0.36925E+01	−0.10758E−01
8	4263168	0.36946E+01	−0.10739E−01	0.36935E+01	−0.10747E−01

Drag and lift coefficients with and without the pressure separation technique.

Table IV. Flow around a 3D cylinder.

		Without pressure separation		With pressure separation	
Level	Cells	C_{drag}	C_{lift}	C_{drag}	C_{lift}
Force					
Reference values: $C_{\text{drag}} \approx 6.185, C_{\text{lift}} \approx 0.00940$					
3	6144	0.59160E+01	−0.12441E−02	0.61155E+01	0.32743E−02
4	49152	0.61549E+01	0.47570E−02	0.61447E+01	0.80229E−02
5	393216	0.61829E+01	0.77422E−02	0.61602E+01	0.91252E−02
6	3145728	0.61861E+01	0.87470E−02	0.61721E+01	0.93316E−02

Lift and drag coefficients with and without the pressure separation technique for $Re = 20$.

This situation changes completely in the case of the flow around the square, in 2D as well as in 3D, which leads to pressure singularities near the corners of the interior square such that the application of pressure separation is getting significantly more advantageous.

Finally, the nonstationary case of a periodically oscillating flow for a medium Reynolds number is also considered and the results are plotted in Figure 5. For the 2D flow around a cylinder, the

DOI: 10.1002/fld

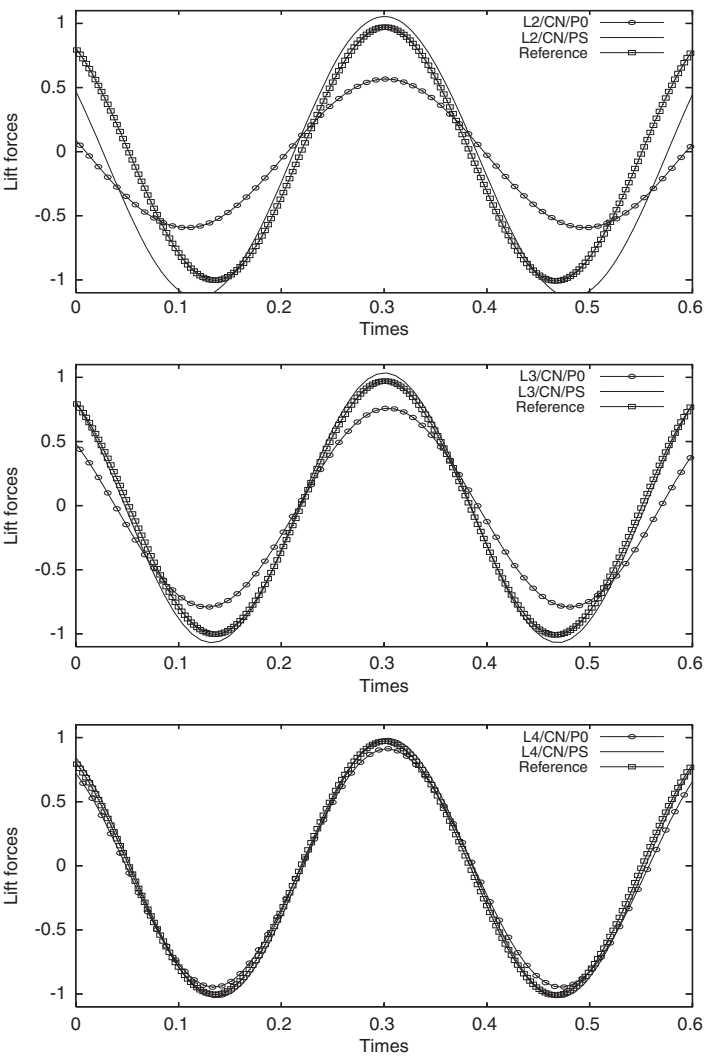

Figure 5. Lift coefficient for various mesh levels ('$L=2$–4') for Crank–Nicolson 'CN' as time-stepping scheme with pressure separation 'PS' and without pressure separation 'P0'.

Reynolds number is increased to $Re=100$, with the aim of examining the resulting effects. The time discretization is based on the classical Crank–Nicolson method, and a fully coupled, fully implicit treatment is used (see [14] for more details). In this nonstationary case, which means the case of higher *Re* number, the PSepA clearly improves the solution for both lift amplitude and frequency. However, since we perform the described constant extrapolation in time only, the results are dependent on the actual time step size too. Hence, more numerical investigations are required to explore the various described variants of the PSepA algorithms to check the numerical behavior w.r.t. accuracy and efficiency.

DOI: 10.1002/fld

3.4. Static bubble

In the next step, we illustrate the robustness and efficiency of the PSepA and of the previously described edge-oriented FEM stabilization in (5), for flows with interfaces, resp., free surfaces, which naturally lead to large pressure derivatives. Owing to its simplicity, but nevertheless due to its prototypical behavior for multiphase flow models, we consider a stationary bubble at equilibrium, something that holds for the slow motion of a gas bubble in a viscoplastic fluid (for instance, see [22]). Since the bubble is at rest, we should have a zero velocity field; unfortunately, most numerical methods generate spurious currents, as, for instance, reported in [11, 12] (see also Figure 2, Tables V and VI).

Table V. Flow around a 2D square.

		Without pressure separation		With pressure separation	
Level	Cells	C_{drag}	C_{lift}	C_{drag}	C_{lift}
Force					
Re = 20/*reference values*: $C_{\text{drag}} \approx 6.47, C_{\text{lift}} \approx 0.0712$					
3	512	0.64522E+01	0.74753E−01	0.68402E+01	0.84024E−01
4	2048	0.63551E+01	0.70146E−01	0.65059E+01	0.73883E−01
5	8192	0.63864E+01	0.69694E−01	0.64587E+01	0.71458E−01
6	32768	0.64239E+01	0.70204E−01	0.64640E+01	0.71122E−01
7	131072	0.64463E+01	0.70646E−01	0.64705E+01	0.71153E−01
8	524288	0.64572E+01	0.70908E−01	0.64728E+01	0.71201E−01
9	2097152	0.64624E+01	0.71039E−01	0.64726E+01	0.71217E−01
Re = 50/*reference values*: $C_{\text{drag}} \approx 4.14, C_{\text{lift}} \approx 0.0239$					
3	512	0.43589E+01	0.31870E−01	0.45827E+01	0.38136E−01
4	2048	0.42174E+01	0.24908E−01	0.42779E+01	0.26107E−01
5	8192	0.41397E+01	0.23774E−01	0.41619E+01	0.24433E−01
6	32768	0.41223E+01	0.23730E−01	0.41385E+01	0.24202E−01
7	131072	0.41248E+01	0.23796E−01	0.41381E+01	0.24102E−01
8	524288	0.41296E+01	0.23830E−01	0.41396E+01	0.24012E−01
9	2097152	0.41328E+01	0.23846E−01	0.41399E+01	0.23951E−01

Drag and lift coefficients with and without the pressure separation technique.

Table VI. Flow around a 3D square.

		Without pressure separation		With pressure separation	
Level	Cells	C_{drag}	C_{lift}	C_{drag}	C_{lift}
Force					
Reference values: $C_{\text{drag}} \approx 7.76, C_{\text{lift}} \approx 0.0688$					
3	8192	0.76277E+01	0.38110E−01	0.77676E+01	0.52552E−01
4	65536	0.77550E+01	0.54334E−01	0.77247E+01	0.63255E−01
5	524288	0.77438E+01	0.63013E−01	0.77342E+01	0.67294E−01
6	4194304	0.77447E+01	0.67372E−01	0.77556E+01	0.68589E−01

Lift and drag coefficients with and without the pressure separation technique for $Re = 20$.

DOI: 10.1002/fld

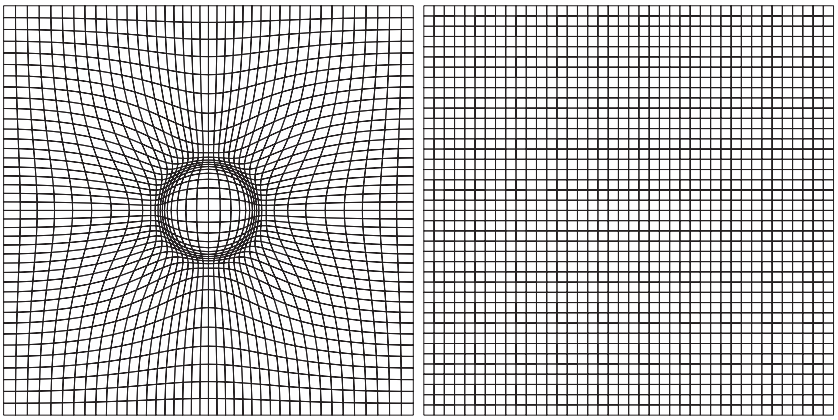

Figure 6. Adapted *vs* 'simple' mesh (both NEL = 1600) on mesh level 4.

In our test case, for the Stokes equations and with exact curvature $1/r$, we restrict the simulation to the configuration proposed in [23, 24], which is a circular bubble with radius $r = 0.25$ positioned in the center of a unit square. The coefficient of surface tension σ and all viscosities were set to unity. Then, according to the Laplace–Young law, the pressure inside the bubble p_i and the outside pressure p_o satisfies

$$p_\mathrm{i} = p_\mathrm{o} + \sigma/r \tag{10}$$

Two different meshes with identical number of mesh cells, and hence degrees of freedom, are considered (see Figure 6), namely an equidistant and a locally adapted mesh by concentrating the grid points in the vicinity of the interface where the pressure exhibits a discontinuity. Consequently, the aligned mesh should resolve the interface in a much better way, while preserving the connectivity of the grid topology for efficiency reasons. Tables VII and VIII show the resulting errors of the velocity and pressure for the different methods, which will be discussed in the subsequent section of this paper.

It is obvious that improved results using the PSepA are mainly obtained for the pressure on the equidistant meshes, whereas on the locally aligned meshes no significant improvements using PSepA are visible since the local alignment itself improves already the pressure error drastically. Moreover, the improvement in the velocity error is almost negligible, particularly to eliminate the spurious currents. Again, the velocity error is significantly improved by adapting the mesh towards the interface using the grid deformation algorithm. Hence, the local grid alignment provides a more precise approximation of the interface, and correspondingly much better results for the pressure, and also for the velocity, are shown in Table VIII. However, the limitation of pressure separation to improve the spurious velocity modes remains: Neither pressure separation nor the grid deformation is able to eliminate totally the spurious velocity.

This is in contrast to the additional (local) stabilization of the momentum equations using the described edge-oriented FEM approach for this type of problems: The results for the velocity improve dramatically, and the error seems to be proportionally decreasing with the order of the mesh-dependent penalty parameter. As a main result, the spurious velocity currents are significantly diminished for both types of meshes. Moreover, increasing the magnitude of the (globally defined)

DOI: 10.1002/fld

Table VII. Equidistant mesh.

	Without pressure separation				With pressure separation			
Level	$\lvert p_i - p_o\rvert/(\frac{\sigma}{r})$	$\lVert\mathbf{u}-\mathbf{u}_h\rVert_0$	$\lvert\mathbf{u}-\mathbf{u}_h\rvert_{1,h}$	NL/MG	$\lvert p_i - p_o\rvert/(\frac{\sigma}{r})$	$\lVert\mathbf{u}-\mathbf{u}_h\rVert_0$	$\lvert\mathbf{u}-\mathbf{u}_h\rvert_{1,h}$	NL/MG
Without edge-oriented FEM								
4	0.954349	0.002608	0.207652	5/1	0.992366	0.001552	0.118638	5/1
5	0.979682	0.000971	0.153784	5/1	0.997579	0.000607	0.091726	5/1
6	0.992961	0.000362	0.112884	4/1	1.001254	0.000237	0.069493	4/1
7	0.997166	0.000138	0.082118	4/1	1.001094	0.000097	0.051485	4/1
With global edge-oriented FEM with penalty parameter $\gamma=10$								
4	0.9520738	3.33E−05	0.002560	6/1	0.989788	2.47E−05	0.001871	6/1
5	0.9792187	1.21E−05	0.001819	5/1	0.997226	9.97E−06	0.001452	5/1
6	0.9926422	4.71E−06	0.001406	5/1	1.001089	3.86E−06	0.001126	5/1
7	0.9966825	1.72E−06	0.001030	4/1	1.000645	1.37E−06	0.000801	4/1
With global edge-oriented FEM with penalty parameter $\gamma=1000$								
4	0.951998	3.38E−07	2.60E−05	6/1	0.988809	2.20E−07	1.64E−05	6/1
5	0.979198	1.23E−07	1.84E−05	5/1	0.997101	8.06E−08	1.16E−05	5/1
6	0.992635	4.78E−08	1.42E−05	5/1	1.001279	3.21E−08	9.07E−06	5/1
7	0.996678	1.75E−08	1.04E−05	4/1	1.000998	1.25E−08	6.46E−06	4/1
With edge-oriented FEM with local penalty parameter γ *as a function of the distance to the interface*								
4	0.949683	3.61E−07	2.68E−05	6/1	0.986366	2.40E−07	1.75E−05	6/1
5	0.978834	1.19E−07	1.73E−05	5/1	0.996440	9.04E−08	1.25E−05	5/1
6	0.992673	4.75E−08	1.31E−05	5/1	1.000876	3.74E−08	9.68E−06	5/1
7	0.996931	2.01E−08	9.56E−06	4/1	1.000757	1.67E−08	6.85E−06	4/1

Errors of pressure and velocity as well as total number of nonlinear iterations and averaged number of multigrid steps per nonlinear iteration (NL/MG) to gain 1 digit.

mesh-dependent penalty parameter does not degrade the performance of the nonlinear, resp., linear, solvers.

Taking into account our previous studies for edge-oriented FEM stabilization [13, 16], in the next step the mesh-dependent penalty parameter is defined not only as a global constant but also as a local function, which takes into account the position of the interface (compare with (5))

$$\sum_{\text{edge E}} \max(\gamma\nu h_E, \gamma^* h_E^2, \gamma_{\text{dist}} f(\text{dist}(\Gamma); h_E) h_E) \int_E [\nabla\mathbf{u}] : [\nabla\mathbf{v}] \, \mathrm{d}s$$

with a sufficiently large constant $\gamma_{\text{dist}} \gg 0$, a distance function dist(Γ) w.r.t. the interface, and f defined as a variant of the Dirac function. Since for problems with free interfaces, the numerical perturbations occur in most cases around the interface, there a high value of the mesh-dependent penalty parameter is required. Away from the interface, the parameters should be designed so that the penalty parameter remains in accordance with the older settings as explained before. Therefore, the mesh-dependent penalty function was defined to be inversely proportional to the distance, which can be obtained, for instance, using a standard level set function as a global distant measure. However, these settings require much more and careful numerical analysis, in particular, in combination with FEM level set techniques for free interface, resp., surface problems, which will be addressed in a forthcoming paper.

DOI: 10.1002/fld

Table VIII. Aligned mesh.

	Without pressure separation				With pressure separation			
Level	$\lvert p_i - p_o\rvert/(\frac{\sigma}{r})$	$\lVert \mathbf{u}-\mathbf{u}_h\rVert_0$	$\lvert \mathbf{u}-\mathbf{u}_h\rvert_{1,h}$	NL/MG	$\lvert p_i - p_o\rvert/(\frac{\sigma}{r})$	$\lVert \mathbf{u}-\mathbf{u}_h\rVert_0$	$\lvert \mathbf{u}-\mathbf{u}_h\rvert_{1,h}$	NL/MG
Without edge-oriented FEM								
4	1.000669	1.89E−04	0.097654	6/1	1.001900	1.74E−04	0.041707	6/1
5	1.000135	3.50E−05	0.057960	5/1	1.000983	5.67E−05	0.032685	5/1
6	1.000032	6.62E−06	0.037825	4/1	1.000322	1.89E−05	0.023153	3/1
7	1.000000	2.25E−06	0.028948	4/1	1.000140	6.48E−06	0.016411	4/1
With global edge-oriented FEM with the penalty parameter $\gamma = 10$								
4	1.000719	1.87E−05	0.004474	5/1	1.000829	1.55E−05	0.003341	5/1
5	1.000336	4.21E−06	0.002285	4/2	1.000513	5.34E−06	0.002529	4/2
6	1.000109	1.66E−06	0.001819	4/2	1.000136	2.05E−06	0.002013	4/2
7	1.000040	5.36E−07	0.001158	4/2	1.000044	6.51E−07	0.001282	4/2
With global edge-oriented FEM with the penalty parameter $\gamma = 1000$								
4	1.000712	2.18E−07	5.11E−05	5/1	1.000650	1.81E−07	3.81E−05	5/1
5	1.000347	5.25E−08	2.71E−05	4/2	1.000465	6.21E−08	2.86E−05	4/2
6	1.000113	2.13E−08	2.19E−05	4/2	1.000119	2.43E−08	2.30E−05	4/2
7	1.000043	6.80E−09	1.37E−05	4/2	1.000035	7.65E−09	1.45E−05	4/2
With edge-oriented FEM with local penalty parameter γ *as a function of the distance to the interface*								
4	1.000599	5.22E−07	1.08E−04	6/1	1.000828	4.95E−07	8.88E−05	5/1
5	1.000277	1.99E−07	8.52E−05	4/2	1.000061	1.72E−07	6.96E−05	4/2
6	0.999927	7.07E−08	6.24E−05	5/2	0.999786	7.31E−08	5.87E−05	5/2
7	1.000017	2.60E−08	4.29E−05	4/2	0.999927	2.46E−08	3.81E−05	4/2

Errors of pressure and velocity as well as total number of nonlinear iterations and averaged number of multigrid steps per nonlinear iteration (NL/MG) to gain 1 digit.

4. CONCLUSION

In this paper we have dealt with the new class of pressure separation algorithms (PSepA) for incompressible flow problems, which may essentially improve the obtained approximation properties of velocity and pressure in such cases where high-pressure derivatives together with small viscosity parameters are dominating the *a priori* error estimate. We extended this concept, which has been recently described in [2] (see also [1] for the 'oldest' description), by several algorithmic concepts, and we provided extensive numerical studies in prototypical flow settings. In particular, for configurations with large pressure gradients due to the geometry or the applied boundary conditions, the theoretical results are confirmed using the resulting numerical tests, for 2D as well as 3D configurations with steady and time-dependent flow behavior. Moreover, we investigated numerically a problem that is prototypical for free interface, resp., multiphase problems where pressure discontinuities and also spurious velocities arise. Although PSepA can essentially improve the pressure approximation, the combination with edge-oriented FEM stabilization seems to eliminate the spurious currents, (almost) independent of the mesh resolution. In this case, the edge-oriented FEM stabilization is applied with a global as well as a local mesh-dependent penalty parameter, which leads to very promising results.

DOI: 10.1002/fld

It is clear that further investigation is necessary to examine some different variations of the PSepA, particularly w.r.t. higher-order finite element spaces or other discretization types, for instance, in the finite volume setting. Moreover, the application of the examined special edge-oriented FEM stabilization to general multiphase problems in conjunction with local mesh adaptation and its interplay with dynamic effects have to be numerically studied and analyzed in future. However, the presented results for the pressure separation algorithms are very promising due to their simplicity and efficiency and also due to their high flexibility regarding very different discretization and solver types, such that much more extensive tests for more realistic flow situations should be performed as soon as possible.

ACKNOWLEDGEMENTS

This work is supported by the German Research Association (DFG) through the collaborative research center SFB/TRR 30 and through the grants TU 102/11-3 (FOR493) and TU 102/21-1.

REFERENCES

1. Schieweck F. *Parallele Lösung der stationären inkompressiblen Navier–Stokes Gleichungen*. Otto-von-Guericke-Universität Magdeburg, Fakultät für Mathematik, 1997 (Habilitation).
2. Ganesan S, John V. Pressure separation: a technique for improving the velocity error in finite element discretisations of the Navier–Stokes equations. *Applied Mathematics and Computation* 2005; **165**:275–290.
3. Girault V, Raviart PA. *Finite Element Methods for Navier–Stokes Equations*. Springer: Berlin, Heidelberg, 1986.
4. Liu J-G, Liu J, Pego RL. Divorcing pressure from viscosity in incompressible Navier–Stokes dynamics. Preprint CSCAMM-05-01, University of Maryland, 2005.
5. Dorok O. Improved accuracy of a finite element discretization for solving the Boussinesq approximation of the Navier–Stokes equations. *Numerical Modelling in Continuum Mechanics* (*Theory*, *Algorithms*, *Applications*), Prague, 22–25 August 1994.
6. Dorok O. Eine stabilisierte Finite-Elemente-Methode zur Lösung der Boussinesq-Approximation der Navier–Stokes–Gleichungen. *Ph.D. Thesis*, Otto-von-Guericke-Universität, 1995.
7. Dorok O, Grambow W, Tobiska L. Aspects of finite element discretizations for solving the Boussinesq approximations. Preprint Math 5/94, Otto-von-Guericke-Universität Magdeburg, 1994.
8. Gerbeau JF, Le Bris C, Bercovier M. Spurious velocities in the steady flow of an incompressible fluid subjected to external forces. *International Journal for Numerical Methods in Fluids* 1997; **25**:679–695.
9. Marianne MF, Sharen JC, Edward DD, Douglas BK, James MS, Matthew WW. A balanced-force algorithm for continuous and sharp interfacial surface tension models within a volume tracking framework. *Journal of Computational Physics* 2006; **213**:141–173.
10. Popinet S, Zaleski S. A front-tracking algorithm for accurate representation of surface tension. *International Journal for Numerical Methods in Fluids* 1999; **30**:775–793.
11. Shirani E, Ashgriz N, Mostaghimi JE. Interface pressure calculation based on conservation of momentum for front capturing methods. *Journal of Computational Physics* 2005; **203**:154–175.
12. Ganesan S, Matthies G, Tobiska L. On spurious velocities in incompressible flow problems with interfaces. *Computer Methods in Applied Mechanics and Engineering* 2007; **196**:1193–1202.
13. Turek S, Ouazzi A. Unified edge-oriented stabilization of nonconforming FEM for incompressible flow problems: numerical investigations. *Journal of Numerical Mathematics* 2007; **15**:299–322.
14. Turek S. *Efficient Solvers for Incompressible Flow Problems*: *An Algorithmic and Computational Approach*. Lecture Notes in Computational Science and Engineering, vol. 6. Springer: Berlin, 1999.
15. Burman E, Hansbo P. A stabilized non-conforming finite element method for incompressible flow. *Computer Methods in Applied Mechanics and Engineering* 2006; **195**:2881–2899.
16. Ouazzi A. *Finite Element Simulation of Nonlinear Fluids. Application to Granular Material and Powder*. Shaker Verlag: Aachen, Germany, 2006. ISBN: 3-8322-5201-0.
17. Bruneau C, Saad M. The 2D lid-driven cavity problem revisited. *Computers and Fluids* 2006; **35**:326–348.

DOI: 10.1002/fld

18. Kalita JC, Shuvam S. The (9, 5) HOC formulation for the transient Navier–Stokes equations in primitive variable. *International Journal for Numerical Methods in Fluids* 2007; **55**:387–406.
19. John V. Higher order finite element methods and multigrid solvers in a benchmark problem for the 3-D Navier–Stokes equations. *International Journal for Numerical Methods in Fluids* 2002; **40**:775–798.
20. Turek S, Schäfer M. Benchmark computations of laminar flow around cylinder. In *Flow Simulation with High-Performance Computers II*, Hirschel EH (ed.), Notes on Numerical Fluid Mechanics, vol. 52. Vieweg: Braunschweig 1996; 547–566. co. Durst F, Krause E, Rannacher R.
21. Braack M, Richter T. Solutions of 3d Navier–Stokes benchmark problems with adaptive finite elements. *Computers and Fluids* 2006; **35**:372–392.
22. Dubash N, Frigaard I. Conditions for static bubbles in viscoplastic fluids. *Physics of Fluids* 2004; **16**:4319–4330.
23. Hysing S. A new implicit surface tension implementation for interfacial flows. *International Journal for Numerical Methods in Fluids* 2006; **51**:659–672.
24. Smolianski A. Numerical modeling of two-fluid interfacial flows. *Ph.D. Thesis*, University of Jyvaskyla, 2001. ISBN: 3-8322-5201-0.

DOI: 10.1002/fld